VELOCITY AND CONCENTRATION PROFILES IN SHEET-FLOW LAYER OF MOVABLE BED

By B. M. Sumer,[1] A. Kozakiewicz,[2] J. Fredsøe,[3] and R. Deigaard[4]

ABSTRACT: Sheet-flow layer of movable bed in steady currents has been investigated experimentally, using four kinds of sediment. Velocity and concentration profiles as well as flow resistance were measured inside and outside the sheet-flow layer. The range of fall-velocity–to–friction-velocity ratio (w/U_f) achieved in the study is $0.2 < w/U_f < 1.7$, which covers both the suspension-mode sediment transport ($w/U_f < 0.8-1$), and the no-suspension-mode sediment transport ($w/U_f > 0.8-1$). In the suspension-mode sheet flow, the flow resistance is found to depend not only on the Shields parameter but also on a parameter involving w. Measured velocity profiles are found to follow the logarithmic law near the bed, outside the sheet-flow layer, whereas inside the sheet-flow layer, they satisfy a power law. Measured concentration profiles, on the other hand, indicate a linear variation with the distance from the bed inside the sheet flow-layer near the bed, whereas away from the bed, the familiar Rouse distribution is satisfied. Evidently, sediment transport in the sheet-flow layer is influenced by the turbulent bursting process.

INTRODUCTION

During recent years, the concept of bed load transport has received renewed attention because comparisons of experimental results and theoretical considerations indicate that the conventional bed-load models are not sufficiently accurate. They have yet to be modified to describe high transport rates more realistically. At high bed shear stresses and sediment transport intensities, the sand waves are washed out and the bed becomes plane. In this regime, the sediment transport near the bed appears to take place in a layer with a thickness being much larger than the grain size. The sediment flow in this layer, which may be termed "sheet flow," is not described properly using the conventional bed-load models.

Earlier measurements in a closed conduit (Wilson 1988, 1989; Wilson and Nnadi 1990; Nnadi and Wilson 1992; Nnadi et al. 1993) have shown that the flow resistance increases drastically with increasing transport intensity in this regime.

Fig. 1 presents the ranges of the relevant flow and sediment parameters in the previous studies plotted together with those of the present study. In the figure, w = the fall velocity of sediment grains and θ = the Shields parameter defined by

$$\theta = \frac{U_f^2}{g(s-1)d} \tag{1}$$

in which U_f = bed friction velocity; s = relative density of sediment grains (ρ_s/ρ), where ρ_s = density of sediment grains and ρ = fluid density; d = grain size; and g = acceleration due to gravity. The curves in the figure represent the identity

$$\frac{w}{U_f} = w^*\theta^{-1/2} \tag{2}$$

in which

$$w^* = \frac{w}{\sqrt{g(s-1)d}} \tag{3}$$

Inspection of Fig. 1 reveals that the extensive data obtained by Wilson and his coworkers show a fairly wide range of θ, although their coverage of the parameter w/U_f is limited, namely $0.3 \lesssim w/U_f \lesssim 0.9$. In a natural flow environment, however, w/U_f may vary over a much wider range.

The purpose of the present work is twofold. One purpose is to complement the study of Wilson and his coworkers by extending the range of w/U_f, thereby investigating the increase in the flow resistance with increasing transport intensity as observed by Wilson. The other is to study other aspects of sheet flows, such as the velocity and concentration profiles inside and outside the sheet-flow layer and concentration time series.

EXPERIMENTAL FACILITY

The experiments were carried out in a tilting flume, 10 m in length, 0.3 m in depth, and 0.3 m in width. Sediment and water were recirculated through the flume. Most of the tests were conducted with a rigidly placed lid to avoid surface waves (duct flow) (Fig. 2). The surface of the lid was hydraulically smooth. Some tests were carried out with a free surface

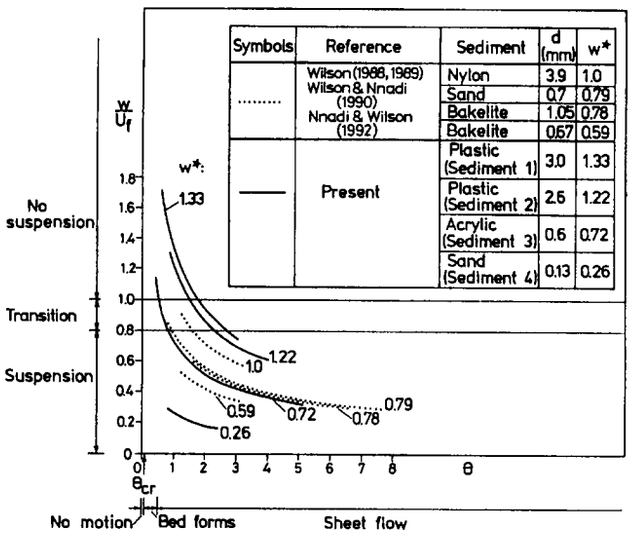

FIG. 1. Ranges of Flow/Sediment Properties (Curves Represent Identity $w/U_f = w^*\theta^{-1/2}$)

[1]Assoc. Prof., Inst. of Hydrodyn. and Hydr. Engrg. (ISVA), Tech. Univ. of Denmark, DK-2800 Lyngby, Denmark.
[2]Visting Res. Engr., Inst. of Hydrodyn. and Hydr. Engrg. (ISVA), Tech. Univ. of Denmark, DK-2800 Lyngby, Denmark; on leave from the Polish Acad. of Sci., Inst. of Hydroengrg., Gdansk, Poland.
[3]Prof., Inst. of Hydrodyn. and Hydr. Engrg. (ISVA), Tech. Univ. of Denmark, DK-2800 Lyngby, Denmark.
[4]Assoc. Prof., Inst. of Hydrodyn. and Hydr. Engrg. (ISVA), Tech. Univ. of Denmark, DK-2800 Lyngby, Denmark.

Note. Discussion open until March 1, 1997. To extend the closing date one month, a written request must be filed with the ASCE Manager of Journals. The manuscript for this paper was submitted for review and possible publication on March 21, 1994. This paper is part of the ***Journal of Hydraulic Engineering***, Vol. 122, No. 10, October, 1996. ©ASCE, ISSN 0733-9429/96/0010-0549–0558/$4.00 + $.50 per page. Paper No. 8081.

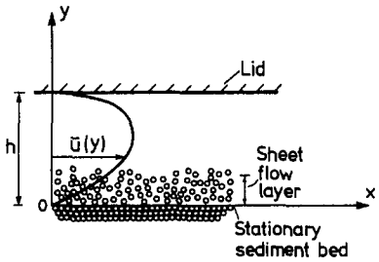

FIG. 2. Definition Sketch Regarding Test Setup (Some Tests Were Conducted without Lid)

flow. The flume had glass side walls, enabling the experimenter to make visual observations of sediment motion.

Four different sediments were used in the tests. The sediment properties are given in Table 1. In the cases of sediment 1 and sediment 2, the use of large grain size made it possible to measure the velocity profile inside the sheet-flow layer, as the thickness of the sheet-flow layer was relatively large. The sediment concentrations can be very high (up to 20%–30%), and the only feasible way of measuring the velocity profile has been the use of a Pitot-tube with a 5 mm outer diameter, which is comparable to the grain size.

Concentration profiles were measured for sediment 3 and sediment 4, using a Delft-Hydraulics conductivity-type concentration meter (CCM). The probe had four electrodes, which can eliminate polarization effect with effective shielding. Concentrations in two-phase flows with grain size $d < 2$ mm can be measured up to 50% by volume. The probe used in the present tests was a wedge-shaped probe. The size of the measurement volume of the probe was $(D_x, D_y, D_z) \cong (0.5$ mm, 1 mm, 6 mm), where x, y, and z are in the streamwise, vertical, and transverse directions, respectively.

RESULTS AND ANALYSIS

Flow Resistance

Flow resistance may be expressed in terms of Nikuradse's equivalent sand roughness, k_s. The k_s values in the present study are calculated using Nikuradse's resistance relation (Schlichting 1979)

$$\frac{U}{U_f} = 2.46 \ln \frac{14.8 r_b}{k_s} \tag{4}$$

in which U = mean flow velocity = $Q/(Bh)$. Here, Q = flow discharge; B = flume width; and h = flow depth. Also, in (4), U_f = bed friction velocity, calculated from

$$U_f = (g r_b I)^{1/2} \tag{5}$$

in which I = energy slope and r_b = hydraulic radius associated with bed. Note that r_b is calculated using the method of Vanoni and Brooks (1957), where the wall correction (for the side walls and, in the present study, for the lid as well) is made.

A total number of 158 tests were performed to determine Nikuradse's equivalent sand roughness, k_s. The test conditions and the end results are given in Table 2. These data were also stored on a diskette, which is obtainable from the Institute of Hydrodynamic and Hydraulic Engineering, Technical University of Denmark (ISVA).

Fig. 3 presents Nikuradse's equivalent sand roughness normalized by the grain size, k_s/d, as a function of the Shields parameter, θ. The low-θ experiments in Fig. 3(c) ($\theta < 0.5$) were undertaken before the bed ripples emerged, therefore no influence of bed waves on the roughness is included here. In the figure, for convenience, the second horizontal axis, based on w/U_f, is also plotted, using (2) and (3). The figure also includes two relations proposed in the literature, i.e., Wilson's (1988, 1989) equation

$$\frac{k_s}{d} = 5\theta \tag{6}$$

and Yalin's (1992) proposed relations

$$\frac{k_s}{d} = 2 \quad (\text{if } \theta < 1) \tag{7}$$

$$\frac{k_s}{d} = 5\theta + (\theta - 4)^2(0.043\theta^3 - 0.289\theta^2 - 0.203\theta + 0.125) \quad (\text{if } 1 < \theta < 4) \tag{8}$$

which resulted from a mathematical fit to Wilson's (1988, 1989) and Wilson and Nnadi's (1990) data. Yalin's relations (7) and (8) are plotted only in Fig. 3(a) to keep the figure relatively simple, while Wilson's $k_s/d = 5\theta$ line is retained in all of the panels as a reference line.

As seen from the figure, the k_s/d versus θ relations for sediments 1 and 2 are similar to those of Wilson (6). The k_s/d versus θ relation for sediment 2 [Fig. 3(b)] matches that of Wilson's nylon rather closely (Fig. 1) and seems to behave in much the same way; therefore, (6) might be a suitable first approximation. The shape of the plotted points for sediments 1 and 2 differs somewhat from (6) but seemingly closely follows the shape of Yalin's relations (7) and (8). The plotted points for sediments 3 and 4, however, differ significantly from (6)–(8).

The variation of k_s/d with θ can be best described by using Figs. 3(b) and 4 for sediment 2. Fig. 4 consists of a sequence of photographs, illustrating the corresponding modes of sediment transport at different stages, as the θ value is increased. The photographs illustrate that the mode of sediment transport changes when a critical value of θ is reached. For example, for the θ values smaller than approximately 2, no suspension

TABLE 1. Sediment Properties

Sediment (1)	Sediment material (2)	Sediment grain size d (mm) (3)	Geometric standard deviation d_{84}/d_{16} (4)	Angle of repose of sediment submerged in water (degrees) (5)	Relative density of sediment grains $s = \rho_s/\rho$ (6)	Fall velocity of sediment grains w (cm/s) (7)	Sediment parameter $w^* = \frac{w}{\sqrt{g(s-1)d}}$ (8)	Remarks (9)
1	Plastic	3.0	Uniform size distribution	26	1.27	11.9	1.33	Circular cylinder with diameter 3 mm and height 3 mm
2	Plastic	2.6	Uniform size distribution	27	1.14	7.3	1.22	Elliptic cylinder with diameters 1.9 mm and 2.8 mm and height 3.3 mm. d = 2.6 mm represents diameter of equivalent circular cylinder with height equal to diameter.
3	Acrylic	0.60	2.3	17	1.13	2.0	0.723	Spherical grains with d_{50} = 0.60 mm
4	Sand	0.13	1.9	23	2.65	1.2	0.262	Natural sand with d_{50} = 0.13 mm

TABLE 2. Flow Resistance Data

Run number (1)	Flow discharge Q (l/s) (2)	Energy slope I ($\times 10^{-3}$) (3)	Flow type (4)	Water depth h (cm) (5)	Mean flow velocity U (cm/s) (6)	Hydraulic radius associated with bed r_b (cm) (7)	Bed friction velocity U_* (cm/s) (8)	Shields parameter θ (9)	Nikuradse's equivalent sand roughness k_s (mm) (10)	k_s/d (11)
					(*a*) Sediment 1					
1	24.50	6.211	F	10.00	81.70	8.10	7.00	0.67	0.740	2.46
2	25.00	15.448	D	8.00	104.17	5.34	9.00	1.02	0.716	2.39
3	26.00	16.213	D	8.19	105.82	5.56	9.40	1.11	0.849	2.83
4	26.00	14.448	D	8.50	101.96	5.75	9.03	1.03	0.863	2.88
5	26.00	6.757	F	10.00	86.70	8.00	7.30	0.72	0.630	2.09
6	26.00	6.757	F	10.00	86.70	8.00	8.00	0.87	0.580	1.94
7	26.50	14.474	D	8.55	103.31	5.75	9.03	1.03	0.815	2.72
8	26.95	14.768	D	8.60	104.46	5.80	9.16	1.06	0.834	2.78
9	27.10	17.574	D	8.12	111.25	5.49	9.72	1.19	0.776	2.59
10	27.50	15.502	D	8.60	106.59	5.83	9.41	1.12	0.865	2.88
11	27.70	19.167	D	8.33	110.84	5.86	10.50	1.39	1.189	3.96
12	28.00	15.847	D	8.68	107.53	5.91	9.59	1.16	0.918	3.06
13	28.00	7.143	F	10.00	93.30	8.00	7.50	0.76	0.530	1.77
14	28.25	21.246	D	8.31	113.32	5.98	11.16	1.57	1.426	4.75
15	28.55	16.064	D	8.74	108.89	5.95	9.68	1.18	0.912	3.04
16	28.75	23.872	D	8.51	112.61	6.39	12.23	1.88	2.241	7.47
17	28.95	24.168	D	8.65	111.56	6.59	12.50	1.97	2.595	8.65
18	29.15	24.825	D	8.55	113.65	6.47	12.55	1.98	2.415	8.05
19	29.45	24.541	D	8.60	114.15	6.49	12.50	1.97	2.345	7.82
20	29.45	15.925	D	8.89	110.42	6.00	9.68	1.18	0.862	2.87
21	29.50	8.264	F	10.00	98.30	8.10	8.10	0.89	0.690	2.31
22	30.10	16.595	D	8.95	112.10	6.09	9.96	1.25	0.927	3.09
23	30.50	17.461	D	8.84	115.01	6.03	10.16	1.30	0.896	2.99
24	30.50	16.819	D	8.86	114.75	5.96	9.92	1.24	0.799	2.66
25	31.10	18.381	D	9.05	114.55	6.34	10.70	1.44	1.208	4.03
26	31.50	9.804	F	10.00	107.00	8.30	8.90	1.08	0.930	3.09
27	31.85	23.151	D	9.51	111.64	7.29	12.87	2.08	3.176	10.59
28	31.95	25.542	D	9.05	117.64	6.87	13.12	2.16	2.652	8.84
29	32.10	19.392	D	9.00	118.89	6.28	10.93	1.50	1.115	3.72
30	32.15	24.247	D	9.17	116.87	6.94	12.85	2.08	2.549	8.50
31	32.40	25.769	D	9.25	116.76	7.09	13.39	2.26	3.034	10.11
32	32.70	25.049	D	9.40	115.96	7.24	13.34	2.24	3.127	10.42
33	33.00	20.777	D	9.24	119.05	6.64	11.63	1.70	1.532	5.11
34	33.25	25.551	D	9.62	115.21	7.50	13.71	2.36	3.644	12.15
35	33.60	26.420	D	9.64	116.18	7.53	13.97	2.46	3.790	12.63
36	34.00	9.804	F	10.00	113.00	8.10	8.80	1.06	0.690	2.30
37	34.00	25.982	D	9.77	116.00	7.63	13.94	2.45	3.838	12.79
38	34.00	24.540	D	9.79	115.76	7.54	13.47	2.28	3.392	11.31
39	34.80	24.804	D	9.76	118.85	7.47	13.48	2.29	3.066	10.22
40	35.60	25.902	D	10.08	117.72	7.87	14.14	2.52	3.952	13.17
41	36.15	26.986	D	10.15	118.72	7.99	14.54	2.66	4.286	14.29
					(*b*) Sediment 2					
42	12.50	7.143	D	6.50	64.10	4.40	5.55	0.86	0.650	2.480
43	13.10	9.541	D	6.50	67.18	4.56	6.53	1.19	1.030	3.960
44	13.65	10.092	D	6.50	70	4.53	6.70	1.26	0.959	3.690
45	14.20	10.637	D	6.56	72.15	4.59	6.92	1.34	0.978	3.760
46	14.50	10	D	7.20	67.10	5	7	1.38	1.100	4.210
47	14.75	11.127	D	6.65	73.93	4.67	7.14	1.43	1.029	3.960
48	15	8.264	D	7	71.40	4.70	6.20	1.07	0.730	2.810
49	15.40	11.652	D	6.90	74.40	4.96	7.53	1.59	1.319	5.070
50	15.95	12.065	D	6.83	77.84	4.82	7.55	1.60	1.083	4.170
51	16.50	12.680	D	6.88	79.94	4.87	7.79	1.70	1.110	4.270
52	16.50	10.309	D	7.30	75.30	5.10	7.20	1.43	0.950	1.430
53	17.05	13.155	D	7	81.19	4.99	8.03	1.81	1.215	4.670
54	17.50	11.494	D	7.50	77.80	5.10	7.60	1.62	0.840	3.250
55	17.60	13.708	D	7.03	83.45	5.03	8.23	1.90	1.207	4.640
56	18	14.239	D	7.35	81.63	5.42	8.70	2.12	1.771	6.810
57	18.20	14.227	D	7.20	84.26	5.20	8.52	2.03	1.383	5.320
58	18.35	14.565	D	7.34	83.33	5.39	8.78	2.16	1.681	6.470
59	18.60	14.820	D	7.46	83.11	5.53	8.97	2.25	1.895	7.290
60	18.85	15.400	D	7.40	84.91	5.49	9.11	2.32	1.836	7.060
61	18.85	15.096	D	7.54	83.33	5.63	9.13	2.34	2.044	7.860
62	19.15	15.504	D	7.70	82.90	5.84	9.42	2.49	2.415	9.290
63	19.20	13.158	D	7.50	85.30	5.40	8.40	1.96	1.420	5.440
64	19.35	15.947	D	7.75	83.23	5.92	9.62	2.59	2.603	10.010
65	19.45	16.127	D	7.66	84.64	5.81	9.58	2.57	2.373	9.130
66	19.50	13.333	D	7.60	85.50	5.40	8.40	1.98	1.290	4.970
67	19.80	16.187	D	7.90	83.54	6.07	9.82	2.70	2.825	10.870
68	19.85	15.767	D	7.84	84.40	5.95	9.59	2.58	2.460	9.460
69	20.15	16.727	D	7.88	85.24	6.05	9.96	2.78	2.762	10.620
70	20.30	16.787	D	7.85	86.20	5.99	9.94	2.77	2.611	10.040
71	20.75	16.906	D	8.10	85.39	6.26	10.19	2.91	3.078	11.840
72	21.30	16.667	D	8.20	86.59	6.29	10.15	2.88	2.907	11.180
73	22.10	16.906	D	8.40	87.70	6.47	10.36	3.00	3.067	11.790
74	22.50	6.667	D	10	78.80	6.20	6.40	1.14	0.610	2.360
75	22.70	17.686	D	8.45	89.55	6.53	10.64	3.17	3.163	12.170
76	23.35	18.225	D	8.70	89.46	6.80	11.03	3.41	3.732	14.360
77	23.50	7.463	D	10.10	77.60	6.30	6.80	1.30	0.610	2.350

TABLE 2. (*Continued*)

(1)	(2)	(3)	(4)	(5)	(6)	(7)	(8)	(9)	(10)	(11)
78	24	18.453	D	9.07	88.20	7.20	11.42	3.65	4.616	17.760
79	24.50	18.798	D	9	90.74	7.09	11.44	3.66	4.176	16.060
80	24.50	17.919	D	9.05	90.24	7.08	11.16	3.49	3.918	15.070
81	24.70	8	D	10.10	81.50	6.30	7	1.38	0.600	2.300
82	25	7.874	D	10.20	81.70	6.40	7	1.38	0.610	2.380
83	25.10	19.797	D	8.90	94.01	6.98	11.65	3.80	3.893	14.970
84	25.15	19.005	D	9.19	91.22	7.28	11.65	3.80	4.465	17.170
85	25.55	20.779	D	9.27	91.87	7.46	12.33	4.26	5.351	20.580
86	25.60	19.491	D	9.31	91.66	7.42	11.91	3.97	4.807	18.490
87	26.05	19.964	D	9.23	94.08	7.31	11.97	4.01	4.429	17.040
88	26.10	8.621	D	10.20	85.30	6.50	7.40	1.55	0.710	2.760
89	26.20	21.775	D	9.26	94.31	7.45	12.62	4.46	5.293	20.360
90	27	8.696	D	10.50	85.70	6.80	7.60	1.63	0.840	3.230
91	27	9.091	D	10.30	87.40	6.60	7.70	1.64	0.810	3.120
92	27	22.074	D	9.43	95.44	7.60	12.83	4.61	5.479	21.070
93	28	9.901	D	10.40	89.70	6.90	8.20	1.88	1.040	4
94	29	8.621	D	10.50	92.10	6.60	7.50	1.56	0.610	2.350
95	29	9.804	D	10.70	90.30	7	8.20	1.89	0.980	3.760
96	29.50	10.638	D	10.50	93.70	7.10	8.60	2.06	1.170	4.510
97	30	10.526	D	10.90	91.70	7.30	8.70	2.12	1.230	4.710
98	30.70	10.638	D	10.50	93	7.40	8.80	2.18	1.330	5.100
99	30.70	11.494	D	10.60	96.50	7.30	9.05	2.29	1.400	5.400
100	31.50	11.905	D	10.70	98.10	7.30	9.25	2.40	1.400	5.400
101	33.30	12.195	D	11	100.90	7.60	9.50	2.54	1.560	6
					(*c*) Sediment 3					
102	9.30	0.643	D	11.30	27.43	5.47	1.86	0.45	0.201	3.350
103	9.40	0.591	D	11.30	27.73	5.04	1.71	0.38	0.103	1.720
104	9.80	0.651	D	11.20	29.17	4.94	1.78	0.41	0.092	1.540
105	10.30	0.797	D	11.40	30.12	5.85	2.14	0.60	0.284	4.730
106	10.30	0.720	D	11.30	30.38	5.16	1.91	0.48	0.119	1.980
107	11.00	1.038	D	11.06	33.15	5.87	2.44	0.78	0.351	5.840
108	11.20	0.891	D	11.30	33.04	5.55	2.20	0.63	0.185	3.080
109	12.10	1.188	D	11.30	35.69	6.21	2.69	0.95	0.419	6.980
110	12.65	1.322	D	11.16	37.78	6.00	2.79	1.02	0.362	6.030
111	13.10	1.217	D	11.45	38.14	5.94	2.66	0.93	0.261	4.350
112	13.45	1.452	D	11.15	40.21	5.93	2.91	1.10	0.318	5.300
113	14.05	1.440	D	11.30	41.45	5.92	2.89	1.09	0.259	4.310
114	14.90	1.755	D	11.25	44.15	6.12	3.25	1.38	0.361	6.010
115	15.05	1.585	D	11.40	44.01	5.96	3.04	1.21	0.248	4.130
116	16.20	2.014	D	11.28	47.87	6.13	3.48	1.58	0.339	5.650
117	16.85	1.980	D	11.50	48.84	6.21	3.47	1.58	0.303	5.050
118	17.50	2.102	D	11.88	49.10	6.67	3.71	1.80	0.456	7.590
119	17.90	2.740	D	10.85	54.99	6.06	4.04	2.13	0.353	5.880
120	18.30	2.464	D	11.35	53.74	6.18	3.87	1.95	0.322	5.370
121	18.75	2.442	D	11.50	54.35	6.30	3.89	1.97	0.317	5.290
122	20.30	2.856	D	11.60	58.33	6.41	4.24	2.35	0.352	5.870
123	20.60	2.804	D	11.55	59.45	6.26	4.15	2.25	0.274	4.560
124	21.50	2.801	D	11.89	60.27	6.30	4.16	2.26	0.258	4.300
125	21.70	3.212	D	11.71	61.77	6.57	4.55	2.71	0.391	6.520
126	22.50	3.239	D	11.80	63.56	6.57	4.57	2.73	0.341	5.680
127	23.00	3.280	D	12.28	62.43	7.10	4.78	2.98	0.519	8.650
128	23.75	3.589	D	12.10	65.43	6.94	4.94	3.19	0.474	7.900
129	23.85	3.788	D	12.06	65.92	7.07	5.13	3.44	0.563	9.380
130	24.25	3.634	D	12.00	67.36	6.79	4.92	3.16	0.384	6.410
131	24.80	3.878	D	12.11	68.26	6.97	5.15	3.46	0.471	7.840
132	26.30	4.039	D	12.30	71.27	7.03	5.28	3.64	0.431	7.180
133	26.90	4.259	D	12.43	72.14	7.22	5.49	3.94	0.514	8.570
134	28.90	4.471	D	12.87	74.85	7.51	5.74	4.31	0.554	9.240
135	29.15	4.775	D	12.81	75.85	7.65	5.98	4.68	0.655	10.920
136	30.00	4.841	D	13.11	76.28	7.93	6.14	4.92	0.749	12.490
137	30.65	5.000	D	13.22	77.28	8.05	6.28	5.16	0.803	13.380
138	31.30	5.262	D	13.47	77.46	8.41	6.59	5.67	1.045	17.420
139	32.00	4.360	D	13.89	76.79	8.01	5.85	4.48	0.573	9.540
					(*d*) Sediment 4					
140	23.50	3.795	D	10.37	75.54	4.68	4.18	0.83	0.044	3.42
141	24.25	3.974	D	10.45	77.35	4.74	4.30	0.88	0.047	3.60
142	25.80	4.790	D	10.32	83.33	4.92	4.81	1.10	0.063	4.88
143	25.90	4.744	D	10.34	83.49	4.86	4.75	1.07	0.057	4.39
144	26.95	5.374	D	10.28	87.39	5.01	5.14	1.26	0.074	5.68
145	27.50	5.774	D	10.16	90.22	5.00	5.32	1.35	0.075	5.78
146	28.85	6.092	D	10.20	94.28	4.92	5.42	1.40	0.062	4.77
147	29.00	6.205	D	10.12	95.52	4.86	5.44	1.41	0.057	4.39
148	29.75	6.769	D	10.13	97.89	5.04	5.78	1.59	0.077	5.90
149	30.90	7.111	D	10.08	102.18	4.90	5.85	1.62	0.060	4.58
150	31.00	7.256	D	10.09	102.41	4.98	5.95	1.69	0.068	5.22
151	32.20	7.726	D	10.08	106.48	4.95	6.13	1.78	0.063	4.82
152	33.00	7.919	D	10.10	108.91	4.91	6.18	1.81	0.056	4.33
153	33.30	7.906	D	10.31	107.66	5.11	6.29	1.88	0.072	5.56
154	34.40	8.436	D	10.30	111.33	5.13	6.51	2.02	0.073	5.61
155	35.70	8.831	D	10.46	113.77	5.29	6.77	2.18	0.085	6.51
156	36.80	8.841	D	10.38	118.18	4.95	6.55	2.04	0.048	3.69
157	37.50	9.192	D	10.40	120.19	5.03	6.73	2.15	0.053	4.04
158	38.40	9.395	D	10.51	121.79	5.11	6.86	2.24	0.056	4.27

Note: Flow type F = free surface flow; flow type D = duct flow.

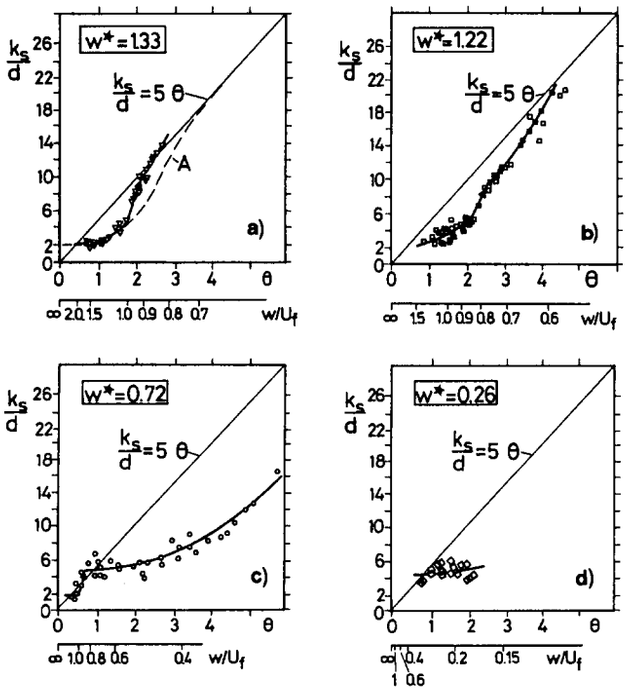

FIG. 3. Variation of k_s/d with θ: (a) Sediment 1; (b) Sediment 2; (c) Sediment 3; (d) Sediment 4 [$k_s/d = 5\theta$ (Wilson 1988, 1989); Curve A (Yalin 1992)]

is observed (all of the grains being transported in the sheet-flow layer), while for θ values larger than 2, the sediment transport also occurs in suspension. It should be noted that the θ value at which suspension begins to occur, namely $\theta \cong 2$, agrees with $w/U_f = 0.8-1$, the range of the critical w/U_f values beyond which grains cannot be kept in suspension, as shown in Fig. 1. For arguments regarding this criterion, see Batchelor (1965) and Bagnold (1966). To illustrate this θ value further, the curve representing the variation of k_s/d with θ, as shown in Fig. 3(b), has a slight jump at the aforementioned critical point. A similar jump is observed in Fig. 3(c), where the roughness, k_s/d, increases with θ in the same way as is shown in Fig. 3(b). However, the jump in k_s/d in Fig. 3(c) (sediment 3) occurs at a much smaller θ value, namely at $\theta \cong 0.6$, which also corresponds to $w/U_f = 0.8-1$. The tests made with sediment 1 reveal a similar relation between k_s/d and θ, as shown in Fig. 3(a). This jump does not occur in the case of sediment 4 [Fig. 3(d)] because the no-suspension-mode sheet-flow regime does not exist in this case; the transport regime changes directly from the suspension-mode regime with bed forms present to the suspension-mode sheet-flow regime (Fig. 1).

Fig. 5(a) depicts the present k_s/d data corresponding to the no-suspension-mode sediment transport, while Fig. 5(b) presents those corresponding to the suspension-mode sediment transport. Regarding the critical value of w/U_f separating the two transport modes, 0.9 was taken in the case of sediment 3 [Fig. 3(c)], 0.8 was taken in the case of sediment 2 [Fig. 3(b)], and 0.95 was taken in the case of sediment 1 [Fig. 3(a)]. Clearly, the critical value of w/U_f is subject to some uncertainty, partly due to the uncertainty related to the critical transport mode itself at this stage and partly due to the uncertainties related to the sediment, such as the grain shape and the grain size distribution. Therefore, the observed differences between the critical values of w/U_f for different sediments may, in fact, be expected.

Sediment encountered in nature may generally be different from the sediment used in the present study. Particularly, the size distribution may not be as uniform as in the present case. The consequence of this would be that, in a real-life situation, the two modes of sediment transport may not be as distinctly defined as those in the present study, since the two modes of sediment transport may occur concurrently for a given grain-size distribution. This implies that, in such a situation, the resistance curves illustrated in Fig. 3 may become smoother.

Fig. 5(b) clearly shows that, in the case of the suspension mode ($w/U_f < 0.8-1$), the roughness depends not only on the Shields parameter θ but also on the parameter w^*. Fig. 5(a), on the other hand, indicates that this is not the case when the sediment is confined in the sheet-flow layer (i.e., in the case of the no-suspension mode, $w/U_f > 0.8-1$). It seems that, in the latter case, the data can be represented by a single curve despite the fairly wide range of w^* tested in the experiments (in fact, the data corresponding to sediments 1 and 2 collapse virtually on the same curve in the interval where the two data

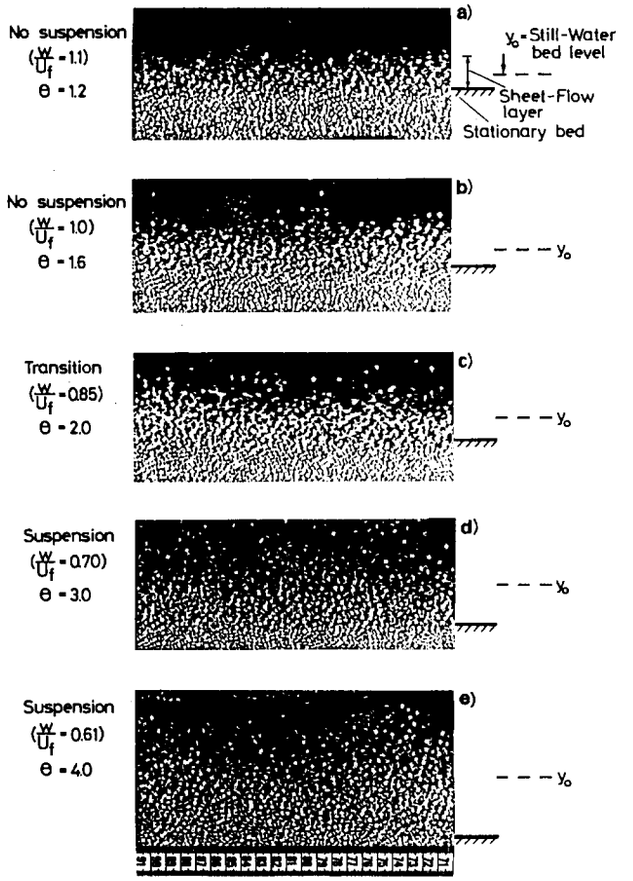

FIG. 4. Sequence Illustrating Transition from "No Suspension" Sheet-Flow Regime to "Suspension" Sheet-Flow Regime for Tests Referred to in Fig. 3(b): (a) θ = 1.2; (b) θ = 1.6; (c) θ = 2.0; (d) θ = 3.0; (e) θ = 4.0

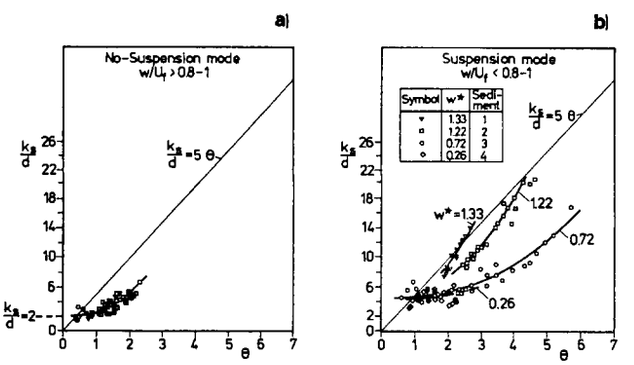

FIG. 5. Variation of k_s/d with θ[$k_s/d = 5\theta$ (Wilson 1988, 1989)]: (a) Solid Line Refers to (9); (b) Solid Lines Refer to (10)

overlap, $0.8 < \theta < 1.7$). Incidentally, the variation of k_s/d with θ in Fig. 5(a) agrees remarkably well with Yalin's equation (8).

Regarding the effect of w^* exhibited in Fig. 5(b), the figure shows that, for a given value of θ, k_s/d decreases with decreasing w^*. This agrees with the observations that the suspended sediment will damp the turbulence, thus leading to a smaller flow resistance. Given the value of θ, the smaller the value of w/U_f, [or, equivalently, the smaller the value of w^* (since $w/U_f = w^*\theta^{-1/2}$)], the larger the amount of sediment transported in suspension; therefore, the larger the damping of turbulence. The flow resistance should decrease with decreasing value of w^*.

For practical purposes, the flow-resistance data in Figs. 5(a) and 5(b) can be represented by the following empirical expressions:

$$\frac{k_s}{d} = 2 + 0.6\theta^{2.5} \quad \text{when } \frac{w}{U_f} > 0.8-1 \tag{9}$$

$$\frac{k_s}{d} = 4.5 + 1.8\exp[0.6(w^*)^4]\theta^{2.5} \quad \text{when } \frac{w}{U_f} < 0.8-1 \tag{10}$$

The latter equation can also be written in the following form, using (2):

$$\frac{k_s}{d} = 4.5 + \frac{1}{8}\exp\left[0.6\left(\frac{w}{U_f}\right)^4\theta^2\right]\theta^{2.5} \quad \text{when } \frac{w}{U_f} < 0.8-1 \tag{11}$$

Fig. 6 shows the k_s/d versus θ data obtained by Wilson (1989) and Wilson and Nnadi (1990) [these data are also listed in Nnadi and Wilson (1992)]. The value of w/U_f corresponding to these data satisfies the criterion $w/U_f < 0.8-1$ over the tested range of θ (Fig. 1), indicating that the suspension mode prevails in Wilson's and Wilson and Nnadi's experiments. The solid lines in Fig. 6 are obtained from the empirical expression given in (10), corresponding to the values of w^* in Wilson's and Wilson and Nnadi's tests.

First, the trend in Fig. 6 is the same as in Fig. 5(b) in that k_s/d for nylon ($w^* = 1.0$) is distinctly larger than that for sand ($w^* = 0.79$) and the bakelites ($w^* = 0.78$ and 0.59).

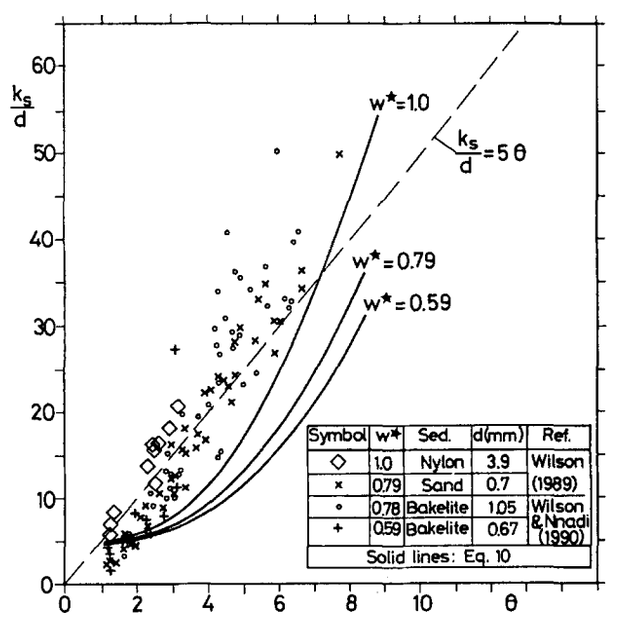

FIG. 6. Comparison of Wilson's and Wilson and Nnadi's Data with Present Results [Only Square Conduit (but Not Round Pipe) Data of Wilson Are Included; Suspension-Mode Sediment Transport ($w/U_f < 0.8 - 1$) Prevails in Wilson's and Wilson and Nnadi's Experiments]

Second, comparison of the present results (the solid curves in the figure) with the Wilson and Wilson and Nnadi data indicates that the present values are somewhat smaller than the Wilson and Wilson and Nnadi values. To see if this is a consequence of the slightly different methods adopted in the two studies, Wilson's results have been recast in terms of the present method [refer to (4) and (5)] using the original data reported in Wilson (1965). The results indicated, however, that the k_s/d values found in this way did not differ much from those given in Wilson (1989). No clear explanation has been found for the observed discrepancy between the present results and the results of Wilson's and Wilson and Nnadi's studies.

Velocity Distribution

Fig. 7 depicts typical velocity profiles measured for sediment 2.

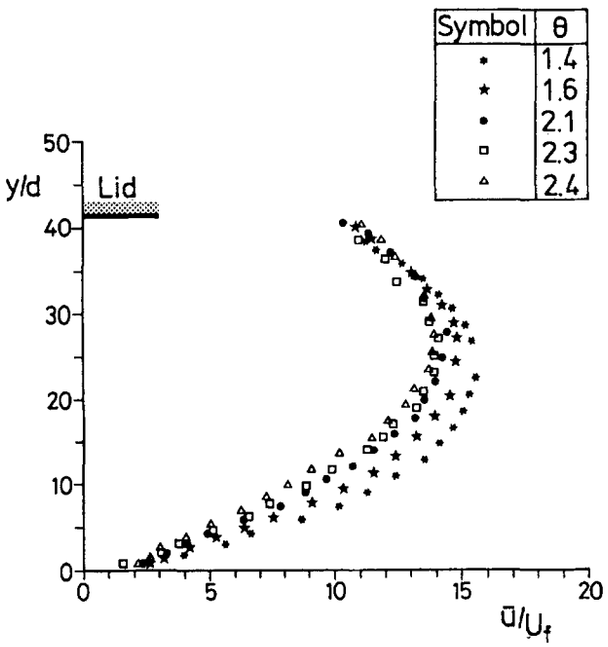

FIG. 7. Measured Velocity Distributions (Sediment 2)

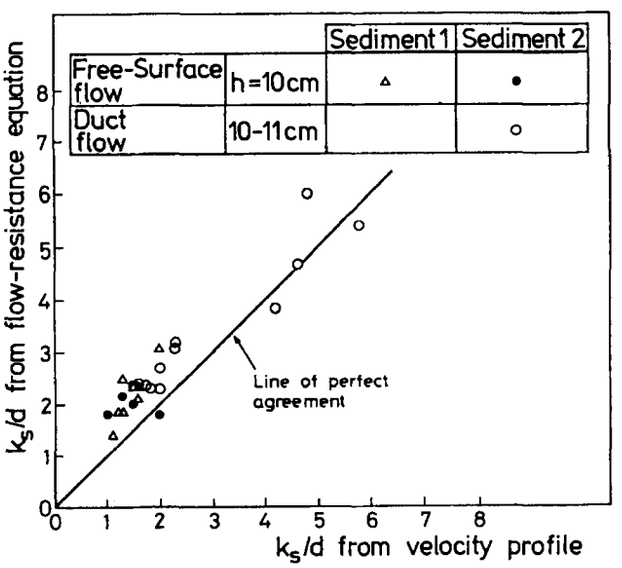

FIG. 8. Comparison of k_s/d Found from Velocity-Profile Measurements [in (12)] with Those Obtained from Flow-Resistance Measurements [in (4)]

Velocity Distribution Outside Sheet-Flow Layer

From similarity considerations, the velocity near the bed but outside the sheet-flow layer may be expected to satisfy the logarithmic law [see, for example, (Rotta 1962, chapter 2, section 11); (Monin and Yaglom 1973, chapter 3, section 5.4)]

$$\frac{\bar{u}}{U_f} = \frac{1}{\kappa} \ln \frac{30(y - \Delta y)}{k_s} \tag{12}$$

provided that the origin of y is shifted by the so-called displacement height, Δy. Here, $\bar{u}$ = mean value of u, the streamwise velocity, at distance y; and κ = Karman constant. The theoretical bed level lies at the origin of $y - \Delta y$.

Given the measured quantities $\bar{u}(y)$ and computing U_f, from (5), and taking κ as 0.407 (=1/2.46), in order to be compatible with (4), the quantities k_s and Δy can be determined from (12). Fig. 8 compares the k_s values calculated in this way with those found from the flow-resistance equation (4), while Fig. 9 presents the results regarding the displacement height Δy. Fig. 10, on the other hand, depicts an example of the velocity profile in a semilogarithmic plot where the y coordinate is shifted, according to Fig. 9.

Fig. 8 indicates that for large values of k_s/d, the two predictions are in fairly good agreement. However, this is not so for small values of k_s/d. The predictions from the velocity

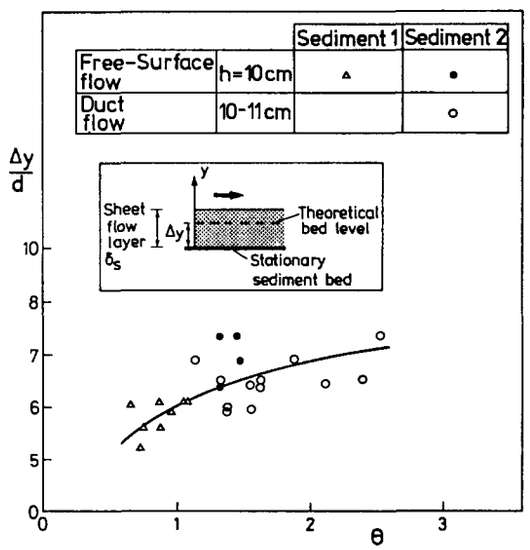

FIG. 9. Displacement Height As Function of θ

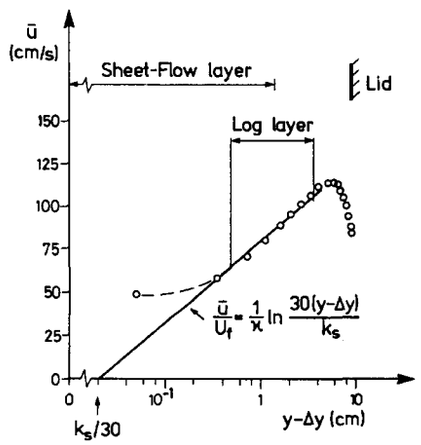

FIG. 10. Comparison of Typical Velocity Distribution with Logarithmic Law near Bed But Outside Sheet-Flow Layer, Sediment 2 (h = 10.3 cm; Q = 27.0 l/s; U = 87.4 cm/s; U_f = 7.7 cm/s; r_b = 6.6 cm; θ = 1.6; Δy = 1.25 cm; δ_s = 2.7 cm)

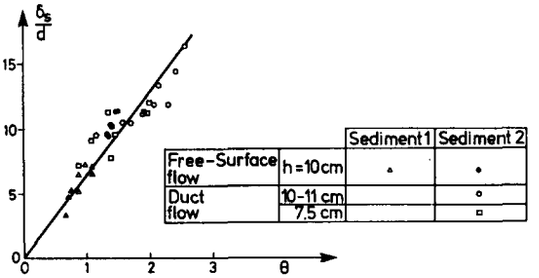

FIG. 11. Thickness of Sheet-Flow Layer Including Tests Presented in Figs. 8 and 9 (from Visual Observation)

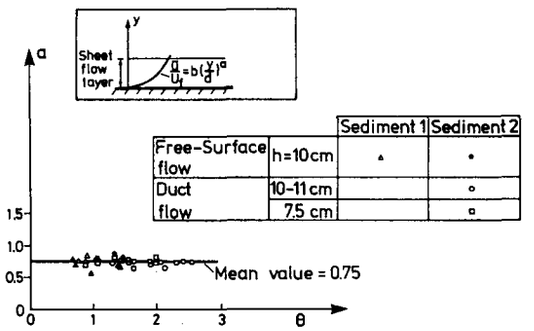

FIG. 12. Power a in Velocity-Distribution Expression (13) As Frunction of θ

profile measurements give 10%–35% smaller values of k_s/d in the latter case. This may be partly due to the particular value of κ adopted (namely, κ = 0.407) in (12) and partly due to the relatively thin logarithmic layer as a result of small flow depth.

Fig. 9 indicates that Δy can take very large values. To compare the calculated values of Δy with the thickness of the sheet-flow layer, δ_s, the latter quantity was measured and the results are plotted in Fig. 11. (Note that the latter data were obtained from visual observations, using the video recordings made during each test, thus subject to some degree of uncertainty. The variation of δ_s with θ will be discussed later under "Concentration Measurements.") Comparison of Figs. 10 and 11 indicates that Δy can be as much as 50% of δ_s and, in some cases, even more. One can draw an analogy between the present flow and the wind flow over vegetation in the atmosphere. It is interesting to note that, for the latter flow with high vegetation, the measured displacement height lies in the range $h_0/2 < \Delta y < h_0$ in which h_0 = the actual height of the vegetation (Monin and Yaglom 1973). As seen, the present results agree quite well with the latter values.

Regarding the velocity profile, Fig. 10 clearly shows that the logarithmic-velocity layer is present near the bed, though it is mostly outside the sheet-flow layer. Apparently, the logarithmic-velocity layer and the sheet-flow layer have an overlapping region, as seen from Fig. 10.

Velocity Distribution in Sheet-Flow Layer

Further analysis of the data reveals that the velocity profile in the major portion of the sheet-flow layer may be expressed in a power form as

$$\frac{\bar{u}}{U_f} = b \left(\frac{y}{d}\right)^a \tag{13}$$

in which the power a apparently remains practically constant, at about 3/4 (Fig. 12), while b decreases with increasing θ (Fig. 13) over the tested range of θ. Hence, (13) may be rewritten as

$$\frac{\bar{u}}{U_f} = b(\theta) \left(\frac{y}{d}\right)^{3/4} \tag{14}$$

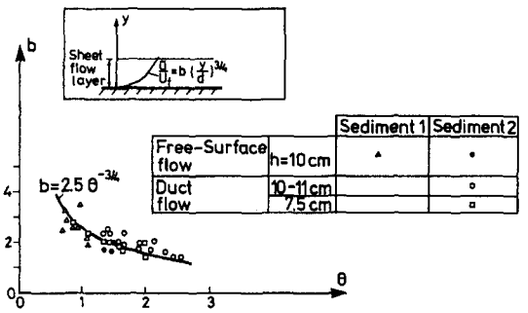

FIG. 13. Coefficient *b* in Velocity-Distribution Expression (14) As Function of θ

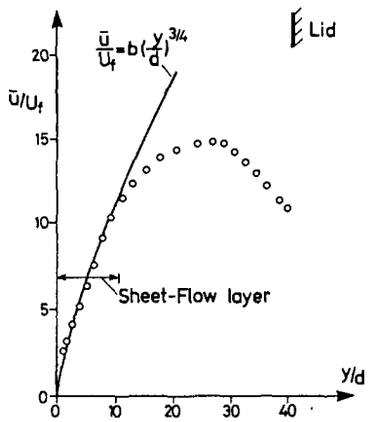

FIG. 14. Comparison of Typical Velocity Distribution with Empirical Power Law in Sheet-Flow Layer. (Same Tests As in Fig. 10; *b* = 2.0)

Fig. 14 gives a typical example of the measured velocity distribution in the sheet-flow layer corresponding to the same test as in Fig. 10.

Returning to (14), the coefficient b, from the data in Fig. 13, can be expressed as

$$b(\theta) = 2.5\theta^{-3/4} \tag{15}$$

and, using Wilson's (1987) expression $\delta_s/d = 10\theta$ (obtained from theoretical considerations related to dynamic friction), (14) may be rewritten in an alternative form

$$\frac{\bar{u}}{U_f} = 14\left(\frac{y}{\delta_s}\right)^{3/4} \tag{16}$$

This implies that y scales better with δ_s than with d. However, we preferred the use of d to that of δ_s in the formulation, as shown in (13), for δ_s is not a well-defined quantity.

Concentration Measurements

Mean Concentration Distribution

Plotted in Figs. 15(a) and 15(b) is the measured time-mean volumetric concentration profile $\bar{c}(y)$ for different values of θ for sediments 3 and 4, respectively. The origin of y is the top of the stationary sediment bed, found by visual observations through the glass side wall of the flume. (The concentration data are available on a diskette, which is obtainable from ISVA).

Figs. 15(a) and 15(b) indicate that $\bar{c}$ varies linearly with y near the bed ($y \lesssim 0.5\ \delta_s$). This agrees with Wilson's (1987) finding.

The linear extensions of the measured concentration profiles for various θs to the bed all point toward $\bar{c} \cong 30\%$. This $\bar{c}$ value is in good agreement with the bed concentration values obtained theoretically by Engelund and Fredsøe (1976).

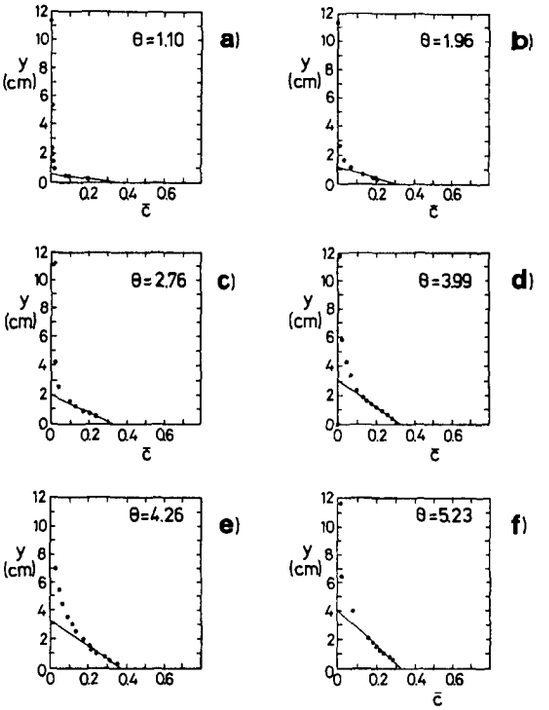

FIG. 15(a–f). Measured Volume-Concentration Profiles with Increasing θ (Sediment 3)

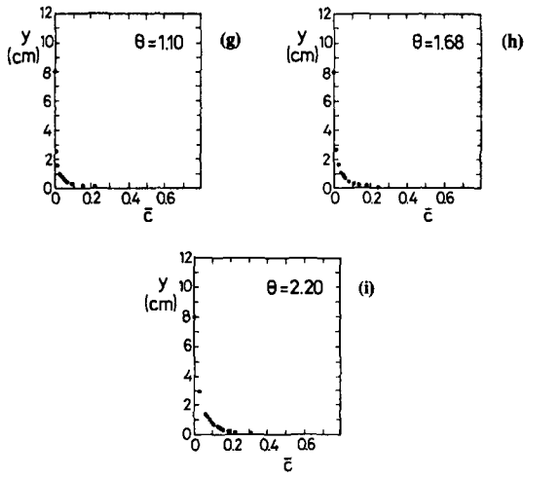

FIG. 15(g–i). Measured Volume-Concentratiion Distribution (Sediment 4)

Fig. 16 compares the thickness of the sheet-flow layer obtained from the measured concentration profiles (see the box in Fig. 16 for the definition sketch) with that obtained from the visual observations with sediments 1 and 2 (Fig. 11). Fig. 16 also includes Wilson's (1987) expression, $\delta_s/d = 10\theta$. Apparently, the prediction from the concentration measurements is slightly larger than that given by the Wilson expression. The δ_s value obtained from $\bar{c}(y)$ profiles differs from that based on the visual observations, which might err due mainly to the negligibly small concentrations far away from the bed.

Fig. 17 compares the measured concentration profile for θ = 4.5 ($w/U_f = 0.3$) with the familiar Rouse (1937) distribution (Vanoni 1975), namely

$$\bar{c} = c_b\left(\frac{h-y}{y}\frac{y_b}{h-y_b}\right)^{w/\kappa U_f} \tag{17}$$

in which y_b = reference distance where concentration is equal to c_b, the reference concentration; and $w/(\kappa U_f)$ = Rouse param-

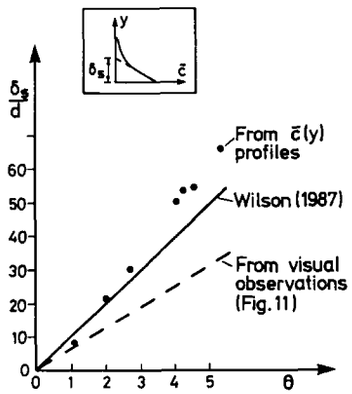

FIG. 16. Comparison of Thickness of Sheet-Flow Layer Obtained from Concentration Profile Measurements (Sediment 3) with That from Visual Observations in Fig. 11 (Sediments 1 and 2) [Solid Line: Wilson's (1987) Expression $\delta_s/d = 10\theta$

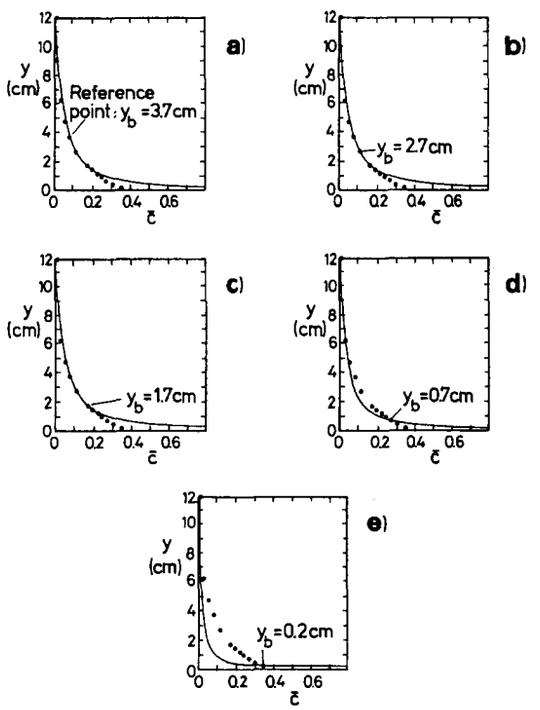

FIG. 17. Comparison of Measured Concentration Profiles with Rouse Distribution (Solid Curves) ($\theta = 4.5$; $w/U_f = 0.34$; Sediment 3): (a) $y_b = 3.7$ cm; (b) $y_b = 2.7$ cm; (c) $y_b = 1.7$ cm; (d) $y_b = 0.7$ cm; (e) $y_b = 0.2$ cm

eter. Comparison is made for different values of reference distance y_b. As shown in Fig. 17, the measured $\bar{c}$ profile agrees rather well with the Rouse distribution for $y > y_b$ when $y_b \geq 1.7$ cm [Figs. 17(a–c)], while they depart from the Rouse distribution when the reference level is taken below that level, namely when $y_b < 1.7$ cm [Figs. 17(d) and 17(e)]. Apparently, it is only when the reference level y_b lies well inside the sheet-flow layer ($y_b \gtrapprox 0.5\ \Delta_s$) that the measured $\bar{c}(y)$ departs from the Rouse distribution. In case of such a small y_b, the upward flux of sediment grains due to turbulent diffusion is no longer able to balance the downward flux due to gravitational fallout. There may be other mechanisms, such as particle-to-particle collision, supporting the grains.

From the preceding considerations, it may be concluded that, for $y \geq y_b \lesssim 0.5\ \delta_s$, the concentration satisfies the Rouse distribution.

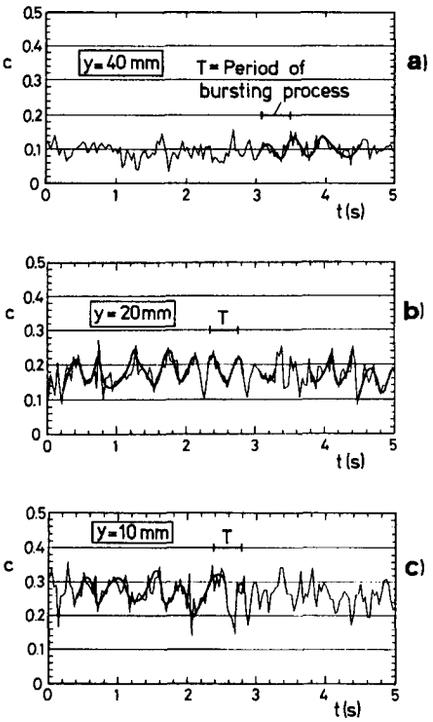

FIG. 18. Samples of Concentration Time Series (Sediment 3; $\theta = 5.2$; $\delta_s \cong 40$ mm; Period of Bursting Process, Calculated from $T = 6\delta/U_0$, Is Indicated): (a) $y = 40$ mm; (b) $y = 20$ mm; (c) $y = 10$ mm

Concentration Time Series

Fig. 18 presents samples of concentration time series taken at three different y locations in one test with sediment 3. The two bottom time series ($y = 10$ and 20 mm) corresponds to y location inside the sheet-flow layer, while the top one ($y = 40$ mm) corresponds to that at the upper edge of the sheet-flow layer. It is evident that the variation of concentration with time shows a periodic behavior. A further analysis of the time series showed that only 30% of the total length of the time series corresponding to $y = 10$ and 20 mm, and an even smaller portion, namely 14%, in the case of $y = 40$ mm, exhibit this kind of behavior. Indicated in Fig. 18 is also the period of the turbulent bursting process (Cantwell 1981), i.e.

$$T = \frac{6\delta}{U_0} \tag{18}$$

in which δ = thickness of boundary layer, taken as $h/2$ in the present case; and U_0 = velocity at free-stream edge of boundary layer, taken as $U_0 = U + 4U_f$, the centerline velocity, adapting Nikuradse's circular pipe expression (Schlichting 1979) as a first approximation. The preceding approximate values of δ and U_0 may be justified, as the main purpose here is to obtain an order of magnitude value for T. As seen from Figs. 18(b) and 18(c), the period of the concentration variations does not differ radically from the indicated value of T. This suggests that the sediment transport in the sheet-flow layer is influenced by the bursting process. [This influence appears to be less pronounced, however, for larger distances from the bed, as suggested in Fig. 18(a)]. The preceding picture is consistent with the results of previous research, investigating the role of turbulent bursting process in suspended-sediment transport (Grass 1983; Sumer 1986; Dyer and Soulsby 1988).

REMARKS ON PRACTICAL APPLICATION

As mentioned previously, the size distribution of sediment encountered in practice is not uniform; therefore, the two

modes of transport, namely the no-suspension and the suspension modes, may not be as clearly defined as in the present study. However, the empirical equations, [(9)–(11)], may still be valid, with the possibility that the critical w/U_f values range a little bit broader than 0.8–1.

Regarding the velocity profile over the bed, $\bar{u}(y)$, the present measurements cover only the case of no-suspension sheet-flow situation. The experimental constraints did not permit us to extend the measurements to also cover the suspension sheet-flow case. Thus, caution must be exercised when (14) is used in the case of suspension transport mode.

CONCLUSIONS

From the present study, several conclusions may be drawn.

1. Flow resistance in the sheet-flow layer can be expressed in terms of the ratio of Nikuradse's equivalent sand roughness to the grain diameter, k_s/d. This ratio behaves differently for two different modes of sediment transport. In the case of no-suspension mode ($w/U_f > 0.8–1$), k_s/d depends on the Shields parameter, θ, only. In the case of suspension mode ($w/U_f < 0.8–1$), however, k_s/d depends not only on θ but also on the parameter $w^* = w/\sqrt{g(s-1)d}$.

In both cases, k_s/d increases with increasing θ. Regarding the dependence of k_s/d on w^*, it increases with increasing w^*.

2. The thickness of the sheet-flow layer, δ_s, increases monotonously with increasing θ.

3 There exists a logarithmic-velocity layer near the bed, though mostly outside the sheet-flow layer, where the velocity distribution satisfies the familiar logarithmic law, provided that the bed level is shifted upward by a distance Δy, which may be as much as 50%–60% or more of δ_s.

4. In the main portion of the sheet-flow layer, the velocity distribution can be represented by a power law [refer to (14)].

5. The concentration distribution within the sheet-flow layer near the bed ($y \lesssim 0.5\ \delta_s$) reveals the linear variation of concentration with the vertical distance from the bed. Away from the bed ($y \gtrsim 0.5\ \delta_s$), however, the concentration satisfies the Rouse distribution.

6. There is evidence that the sediment transport in the sheet-flow layer is influenced by the turbulent bursting process.

ACKNOWLEDGMENTS

This work was funded jointly by the Danish Technical Research Council (STVF) under the program "Marin Teknik" and by the Commission of the European Communities, Directorate General for Science, Research and Development, under MAST contracts No. 0035-C and MAS 2 CT 92-0027. Mr. Zhen Ming Wang (research engineer) conducted the experiments related to the velocity-distribution measurements.

APPENDIX I. REFERENCES

Bagnold, R. A. (1966). "An approach to the sediment transport problem from general physics." *Profl. Paper No. 422-I*, U.S. Geological Survey, U.S. Govt. Printing Ofc., Washington, D.C.

Batchelor, G. K. (1965). "The motion of small particles in turbulent flow." *Proc., 2nd Australian Conf. on Hydr. and Fluid Mech.*, Univ. of Auckland, Auckland, Australia, 019–041.

Cantwell, B. J. (1981). "Organized motion in turbulent flow." *Ann. Rev. Fluid Mech.*, 13, 457–515.

Dyer, K. R., and Soulsby, R. L. (1988). "Sand transport on the continental shelf." *Ann. Rev. Fluid Mech.*, 20, 295–324.

Engelund, F., and Fredsøe, J. (1976). "A sediment transport model for straight alluvial channels." *Nordic Hydro.*, 7, 293–306.

Grass, A. J. (1983). "The influence of boundary layer turbulence on the mechanics of sediment transport." *Proc., Euromech 156/Mech. of Sediment Transport*, A. A. Balkema, Rotterdam, The Netherlands, 3–17.

Monin, A. S., and Yaglom, A. M. (1973). *Statistical fluid mechanics: mechanics of turbulence*. MIT Press, Cambridge, Mass.

Nnadi, F. N., and Wilson, K. C. (1992). "Motion of contact-load particles at high shear stress." *J. Hydr. Engrg.*, ASCE, 118(12), 1670–1684.

Nnadi, F. N., Shaw, J. K., and Wilson, K. C. (1993). "Sheet-flow transport by unidirectional motion and asymmetric waves." Can. Coastal Engrg. Conf., Vancouver, Canada.

Rotta, J. C. (1962). "Turbulent boundary layers in incompressible flow." *Progress in aeronautical sciences*, A. Ferri, D. Küchemann, and L. H. G. Sterne, eds., The Macmillan Company, New York, N.Y., 5–212.

Rouse, H. (1937). "Modern conceptions of the mechanics of fluid turbulence." *Trans.*, ASCE, New York, N.Y., 102, 463–543.

Schlichting, H. (1979). *Boundary-layer theory*. McGraw-Hill Book Co., Inc., New York, N.Y.

Sumer, B. M. (1986). "Recent developments on the mechanics of sediment suspension." *Transport of suspended solids in open channels*, W. Bechteler, ed., A. A. Balkema, Rotterdam, The Netherlands, 3–22.

Vanoni, V. A. (1975). *Sedimentation engineering*. ASCE Manuals and Rep. on Engrg. Pract., 54, ASCE, New York, N.Y.

Vanoni, V. A., and Brooks, N. H. (1957). "Laboratory studies of the roughness and suspended load of alluvial streams." Caltech Sedimentation Lab., Pasadena, Calif., M.R.D. Sediment Ser. No. 11.

Wilson, K. C. (1965). "Derivation of regime equations from relationships for pressurized flow by use of the principle of minimum energy-degradation rate," PhD thesis, Queen's Univ., Kinston, Ontario, Canada.

Wilson, K. C. (1987). "Analyses of bed-load motion at high shear stress." *J. Hydr. Engrg.*, ASCE, 113(1), 97–103.

Wilson, K. C. (1988). "Frictional behaviour of sheet flow." *Prog. Rep. No. 67*, Inst. of hydrodyn. and Hydr. Engrg., Technical Univ. of Denmark, DK-2800 Lyngby, Denmark, 11–22.

Wilson, K. C. (1989). "Mobile bed friction at high shear stress." *J. Hydr. Engrg.*, ASCE, 115(6), 825–830.

Wilson, K. C., and Nnadi, F. N. (1990). "Behaviour of mobile beds at high shear stress." *Proc., 22nd Coastal Engrg. Conf.*, ASCE, New York, N.Y., 3, 2536–2541.

Yalin, M. S. (1992). *River Mechanics*. Pergamon Press, Inc., Tarrytown, N.Y.

APPENDIX II. NOTATION

The following symbols are used in this paper:

a = power in velocity distribution (14);
B = width of flume;
b = coefficient in velocity distribution (14);
c = concentration;
$\bar{c}$ = time-mean concentration;
c_b = reference concentration;
$D_{x,y,z}$ = size of measurement volume of concentration probe in x-, y-, and z-directions;
d = grain size;
g = acceleration due to gravity;
h = flow depth;
I = energy slope;
k_s = Nikuradse's equivalent sand roughness;
Q = flow discharge;
r_b = hydraulic radius associated with bed;
s = relative density of sediment grains = ρ_s/ρ;
T = period of bursting process;
t = time;
U = mean flow velocity = $Q/(Bh)$;
U_f = bed friction velocity;
U_0 = velocity at free-stream edge of boundary layer or centerline velocity in pipe or duct flow;
u = velocity in streamwise direction;
$\bar{u}$ = time mean velocity in streamwise direction;
w = fall velocity of sediment grains;
w^* = parameter $w^* = w/\sqrt{g(s-1)d}$;
x = streamwise distance;
y = distance from stationary bed;
y_b = reference distance;
z = transverse distance;
Δy = displacement height;
δ = boundary-layer thickness;
δ_s = thickness of sheet-flow layer
θ = Shields parameter;
κ = Karman constant;
ν = kinematic viscosity;
ρ = fluid density;
ρ_s = density of sediment grains; and
$\bar{(\ )}$ = time mean.